Thermodynamic properties of massive dilaton black holes II

Takashi Tamaki*

Department of Physics, Waseda University, Ohkubo, Shinjuku, Tokyo 169-8555, Japan

(February 7, 2008)

We numerically reanalyze static and spherically symmetric black hole solutions in an Einstein-Maxwell-dilaton system with a dilaton potential $m_d^2\phi^2$. We investigate thermodynamic properties for various dilaton coupling constants and find that thermodynamic properties change at a critical dilaton mass $m_{d,crit}$. For $m_d \geq m_{d,crit}$, the black hole becomes an extreme solution for a nonzero horizon radius $r_{h,ex}$ as the Reissner-Nordström black hole. However, if m_d is nearly equal to $m_{d,crit}$, there appears a solution of smaller horizon radius than $r_{h,ex}$. For $m_d < m_{d,crit}$, a solution continues to exist until the horizon approaches zero. The Hawking temperature in the zero horizon limit resembles that of a massless dilaton black hole for arbitrary dilaton coupling constant.

04.40.-b, 04.70.-s, 95.30.Tg. 97.60.Lf.

I. INTRODUCTION

The black hole solution in the Einstein-Maxwell-dilaton system found by Gibbons and Maeda, and independently by Garfinkle, Horowitz and Strominger (GM-GHS) has many distinctive properties from those of the conventional Reissner-Nordström (RN) black hole [1]. Among the most important are its thermodynamic properties. If we consider the evaporation process of the black hole, its final fate varies depending on the dilaton coupling.

For dilaton couplings $\gamma < 1$, the Hawking temperature approaches zero by reducing the mass, while it diverges for dilaton couplings $\gamma > 1$ in the zero horizon limit [2]. For the intermediate value $\gamma = 1$, the temperature remains finite and nonzero in this limit.

These facts tell us that the scalar field plays a role in determining the properties of black holes. It is worth mentioning that hairy black holes [3–5] which have a Yang-Mills field and a Higgs field also change qualitatively when scalar hair such as a Brans-Dicke scalar field is added [6].

However, since the dilaton field has been predicted to have a TeV scale mass and a massless dilaton field is excluded by experimental considerations [7], we need to investigate black hole solutions with a massive dilaton field as a more realistic case. Several authors have discussed this possibility and found some interesting prop-erties [8]. For example, these black holes may have three horizons, or wormholes outside the event horizon in the string metric near the extreme solution for the magnetically charged solution. However, since the inclusion of a mass term makes it hard to obtain a solution in closed analytic form, there remains some room for further investigation [9].

We have investigated previously the thermodynamic properties of these black holes for the particular dilaton coupling $\gamma = 1$ [11]. However, the value of the dilaton coupling is not fixed experimentally. Moreover, theoretical considerations do not necessarily favor a dilaton coupling equal to 1. For example, $\gamma = \sqrt{3}$ is suggested by a four-dimensional effective model obtained from the five-dimensional Kaluza-Klein theory.

We therefore concentrate here on studying the dependence of the dilaton couplng and clarify some aspects which have not been investigated so far.

This paper is organized as follows. In Sec. II, we describe our model, basic equations and boundary conditions. We briefly review the GM-GHS solution in Sec. III. Our main results are given in Sec. IV and V, with concluding remarks in Sec. VI. Throughout this paper, we use the units $G = c = \hbar = 1$.

II. BASIC EQUATIONS

We take the action as follows,

$$S = \int d^4x\sqrt{-g}\left[R - 2(\nabla\phi)^2 - e^{-2\gamma\phi}F^2 - 2V(\phi)\right], \quad (1)$$

where ϕ, γ and $V(\phi)$ are a dilaton field, its coupling constant and its potential, respectively. The Einstein equations, the dilaton equation and the Maxwell equation are

$$G_{\mu\nu} = 2\left(\nabla_\mu\phi\nabla_\nu\phi + e^{-2\gamma\phi}F_\mu^\lambda F_{\nu\lambda}\right)$$
$$-g_{\mu\nu}\left[(\nabla\phi)^2 - \frac{1}{2}e^{-2\gamma\phi}F^{\alpha\beta}F_{\alpha\beta} - V\right], \quad (2)$$

$$\Box\phi + \frac{\gamma}{2}e^{-2\gamma\phi}F^{\mu\nu}F_{\mu\nu} - \frac{1}{2}\frac{dV(\phi)}{d\phi} = 0, \quad (3)$$

$$\nabla_\mu F^{\mu\nu} - 2\gamma(\nabla_\mu\phi)F^{\mu\nu} = 0. \quad (4)$$

We consider the static and spherically symmetric metric as

$$ds^2 = -f(r)e^{-2\delta(r)}dt^2 + f(r)^{-1}dr^2 + r^2d\Omega^2, \quad (5)$$

where $f(r) := 1 - 2m(r)/r$. We choose a gauge potential A_μ as

---

*electronic mail :tamaki@gravity.phys.waseda.ac.jp

$$A_\mu = (A(r), 0, 0, Q_m \cos\theta), \tag{6}$$

where Q_m is a magnetic charge. We do not consider a dyonic black hole which has both an electric and a magnetic charge here. Below, we consider a dilaton potential $V = m_d^2 \phi^2$ where m_d is the dilaton mass, for simplicity. In this case, the boundary conditions at spatial infinity to satisfy asymptotic flatness are

$$m(\infty) =: M = const., \quad \delta(\infty) = 0, \quad \phi(\infty) = 0. \tag{7}$$

From the Maxwell equation, we obtain

$$(rK)' + K = 0, \tag{8}$$

where $' := d/dr$ and $K := A' e^{-2\gamma\phi + \delta}$. By integrating this equation, we obtain

$$r^2 K = const. =: Q_e. \tag{9}$$

Q_e can be interpreted as electric charge because of the condition (7). Finally, our basic equations are

$$m' = \frac{r^2}{2} \left(f\phi'^2 + B + V \right), \tag{10}$$

$$\delta' = -r\phi'^2, \tag{11}$$

$$A' = \frac{Q_e}{r^2} e^{2\gamma\phi - \delta}, \tag{12}$$

$$\phi'' + \frac{2\phi'}{r} + \frac{1}{f} \left[\phi' \left\{ \frac{2m}{r^2} - r(B+V) \right\} \right.$$
$$\left. + \gamma \left(\frac{Q_m^2}{r^4} e^{-2\gamma\phi} - \frac{Q_e^2}{r^4} e^{2\gamma\phi} \right) - \frac{1}{2}\frac{dV}{d\phi} \right] = 0, \tag{13}$$

where we use the abbreviation

$$B := \frac{Q_m^2}{r^4} e^{-2\gamma\phi} + \frac{Q_e^2}{r^4} e^{2\gamma\phi} . \tag{14}$$

We also assume the existence of a regular event horizon at $r = r_h$. So we have

$$m_h = \frac{r_h}{2}, \quad \delta_h < \infty, \quad \phi_h < \infty, \tag{15}$$

$$\phi'_h = \frac{r(dV_h/d\phi - 2\gamma B_h)}{2\{1 - r_h^2(B_h + V_h)\}}. \tag{16}$$

The variables with subscript h are evaluated at the horizon. We will obtain the black hole solution numerically by determining ϕ_h iteratively to satisfy these conditions.

III. THE GM-GHS SOLUTION

We briefly describe the GM-GHS solution, i.e., the massless dilaton black hole, to compare with the massive dilaton black hole. To describe the exact solution, it is convenient to use the following spherically symmetric ansatz:

$$ds^2 = -\lambda^2 dt^2 + \frac{1}{\lambda^2} dr^2 + R^2 d\Omega^2 , \tag{17}$$

where λ and R are functions of r only.

We consider the electrically charged case. Since this system has an electric-magnetic duality $F \to e^{-2\phi}\tilde{F}$, $\phi \to -\phi$, we can easily obtain the results for the magnetically charged case. With the above ansatz, we obtain

$$e^{2\phi} = \left(1 - \frac{r_-}{r}\right)^{2\gamma/(1+\gamma^2)} , \tag{18}$$

$$\lambda^2 = \left(1 - \frac{r_+}{r}\right)\left(1 - \frac{r_-}{r}\right)^{(1-\gamma^2)/(1+\gamma^2)} , \tag{19}$$

$$R = r\left(1 - \frac{r_-}{r}\right)^{\gamma^2/(1+\gamma^2)} , \tag{20}$$

where we have set the asymptotic value of the dilaton field to zero. r_+ and r_- are the event horizon and the inner horizon, respectively. They are related to the gravitational mass M and charge Q_e by

$$M = \frac{r_+}{2} + \left(\frac{1-\gamma^2}{1+\gamma^2}\right)\frac{r_-}{2} , \tag{21}$$

$$Q_e = \left(\frac{r_+ r_-}{1+\gamma^2}\right)^{1/2} . \tag{22}$$

The above solution has many interesting features, one of which is that the inner horizon is singular and this singularity is spacelike for any nonzero value of γ. The second feature is thermodynamical. Temperature T is written as

$$T = \frac{1}{4\pi r_+} \left(1 - \frac{r_-}{r_+}\right)^{\frac{1-\gamma^2}{1+\gamma^2}} . \tag{23}$$

This vanishes in the zero horizon area limit for $\gamma < 1$, whereas it has a finite value $1/(8\pi M)$ for $\gamma = 1$ and diverges for $\gamma > 1$ in the same limit. Thus, these differences are caused by the dilaton field and to examine this feature for the massive dilaton black hole is one of our basic motivations.

IV. PROPERTIES OF THE MASSIVE DILATON BLACK HOLE

First, we summarize the results of previous papers which do not depend on the dilaton potential V whenever V is convex [8]: (i) The dilaton is monotonically increasing (decreasing) outside the horizon for the electrically (magnetically) charged solution. (ii) For $Q_e m_d \lesssim 1$ (or $Q_m m_d \lesssim 1$), there can be only one horizon. In previous papers only the case $\gamma = 1$ is considered, but it is trivial to extend the above results to arbitrary γ.

When V is an even function, we can also obtain results for the magnetically charged case from the electrically charged case by means of the electric-magnetic duality

mentioned above. Consider for example the magnetically charged solutions with $Q_m = 0.1$.

First, we consider the intrinsic difference of the dilaton field with a mass term from that of the massless dilaton field in an asymptotic region. For the GM-GHS solution, the dilaton field goes as $e^{-2\phi} \sim 1 + 2\Sigma/r$ in the asymptotic region, where Σ is a dilaton charge. The latter is expressed as

$$\Sigma = -\frac{Q_m^2}{2M} .\tag{24}$$

This is known as a secondary charge since it is completely determined by the gravitational mass and the magnetic charge.

On the contrary, for the massive dilaton black hole, the dilaton field behaves as $\phi \sim \gamma Q_m^2/m_d^2 r^4$ [8] since Eq. (13) can be approximated as

$$\gamma \frac{Q_m^2}{r^4} = \frac{1}{2}\frac{dV}{d\phi},\tag{25}$$

by neglecting the derivative terms of ϕ in the asymptotic region. Thus, the dilaton charge is lost because of the dilaton potential.

We show the behavior of the dilaton field outside the horizon for horizon radii $r_h = 0.15$ and 0.05, dilaton mass $m_d = 10$ and dilaton coupling $\gamma = 1$ in Fig. 1 (solid lines). For comparison, we also show those of the GM-GHS solution and the approximate solution $\phi = \gamma Q_m^2/m_d^2 r^4$ (dotted lines and dashed lines, respectively.).

It is seen that the deviation from the approximate solution becomes large for $r_h = 0.05$ compared with that for $r_h = 0.15$. This is related to the fact that the massive dilaton field behaves like a massless one within its Compton wavelength scale $\sim 1/m_d$.

On the other hand, since the influence of the dilaton field becomes negligible for $r \gtrsim 1/m_d$, the solution is expected to approach the RN solution for large m_d or large horizon radius. Thus, we may expect a qualitative difference depending on the scale of the horizon radius.

This behavior may influence other structures. Actually, a wormhole structure outside the event horizon in the string metric near the extreme black hole of the magnetically charged case, which is absent for the GM-GHS solution, is reported in Ref. [8].

Next, we turn our attention to sequences of solutions, corresponding to various horizon radii. We analyze the conditions for the existence of a degenerate horizon along the same lines as Ref. [8]. If the horizon becomes degenerate at $r = r_d$, we have $m' = 1/2$ at the horizon, which leads to

$$1 = \frac{Q_m^2 e^{-2\gamma\phi_d}}{r_d^2} + m_d^2\phi_d^2 r_d^2,\tag{26}$$

from Eq.(10). Note that we can rewrite Eq.(13) by using Eq.(10) as

$$f\left(\phi'' + \frac{2\phi'}{r}\right) + \phi'(f' + rf\phi'^2)$$
$$+\frac{\gamma Q_m^2}{r^4}e^{-2\gamma\phi} - m_d^2\phi = 0.\tag{27}$$

Then, by using $f_d = f_d' = 0$, we have

$$0 = \frac{\gamma Q_m^2 e^{-2\gamma\phi_d}}{r_d^2} - m_d^2\phi_d r_d^2.\tag{28}$$

Note that the finiteness of ϕ_d and ϕ_d' at $r = r_d$ are assumed implicitly. From these conditions, we obtain

$$\frac{1}{\phi_d(\phi_d + 1/\gamma)m_d^2} = r_d^2,\tag{29}$$

$$\frac{e^{2\gamma\phi_d}}{\phi_d(\phi_d + 1/\gamma)^2} = \gamma Q_m^2 m_d^2.\tag{30}$$

As we mentioned at the begining of this section, ϕ_d is restricted to $\phi_d > 0$ since the dilaton is monotonically decreasing outside the horizon for the magnetically charged case. Thus, the left-hand side of Eq. (30) reaches its minimum value $e^2\gamma^3/4$ at $\phi_d = 1/\gamma$. [Note that e here refers not to electric charge but to the Euler number $e = 2.71\cdots$.]

Thus, the solution for $Q_m^2 m_d^2 < e^2\gamma^2/4$ does not have an extreme limit, *if ϕ_d and ϕ_d' have finite values.* To check this, we find the solutions numerically. Let us denote the dilaton mass which satisfies $Q_m^2 m_d^2 = e^2\gamma^2/4$ by $m_{d,crit}$. For $\gamma = 0.5$, 1 and $\sqrt{3}$, we find that $m_{d,crit}$ takes values $6.79\cdots$, $13.59\cdots$ and $23.54\cdots$, respectively. We pay attention to the qualitative difference depending on the dilaton mass.

The horizon radius r_h and the inverse temperature $1/T$ are shown in terms of the gravitational mass M of the massive dilaton black hole for the case $\gamma = 1$ in Figs. 2 (a) and (b), respectively (solid lines). We also show the GM-GHS and the RN solutions with a dotted line and a dashed line, respectively.

The relationship between the extreme solution and the zero temperature is directly connected to the first law of black hole thermodynamics. If we fix the magnetic charge, it can be expressed as

$$\frac{dr_h}{dM} = \frac{1}{2\pi r_h T} .\tag{31}$$

Since dr_h/dM approaches infinity in the extreme limit for nonzero r_h in the RN solution, T approaches zero. On the other hand, for the GM-GHS solutions with $\gamma = 1$, since dr_h/dM diverges as r_h approaches zero, T can remain finite.

For massive dilaton black holes, our calculation shows that there are two distinct cases, depending on the dilaton mass. For $m_d > m_{d,crit}$, there is an extreme solution for nonzero horizon radius. For $m_d < m_{d,crit}$, the solution continues to exist in the $r_h \to 0$ limit where

T remains finite nonzero value, as in the corresponding GM-GHS solution. We defer discussion of the case $m_d = m_{d,crit}$ to the next section.

We also show the corresponding diagrams for $\gamma = 0.5$ and $\sqrt{3}$ (suggested by Kaluza-Klein theory) in Figs. 3 (a) and (b), and in Figs. 4 (a) and (b), respectively. Note that the solution in these cases also becomes an extreme one for a nonzero horizon radius with $m_d > m_{d,crit}$, as in the case $\gamma = 1$ discussed above. Thus, in some respects these diagrams are similar to the case $\gamma = 1$.

It is surprising that the temperature in the zero horizon limit for $m_d < m_{d,crit}$ closely resembles that of the GM-GHS solution. I.e., the temperature diverges, approaches zero or has a finite nonzero value in the zero horizon limit, according as $\gamma > 1$, $\gamma < 1$ or $\gamma = 1$, respectively. We confirmed this result for various γ. This is also related to the fact that the dilaton field behaves like a massless field within its Compton wavelength. However, since the mass term of the dilaton field affects the gravitational mass even in the zero horizon limit, the solution itself is quite different from the GM-GHS solution. Thus, it is not trivial whether or not the temperature of a massive dilaton black hole in the zero horizon limit resembles that of the GM-GHS solution qualitatively.

In previous papers [8], it was shown that a necessary condition for the existence of three horizons is the violation of the strong energy condition (SEC). In our example, the violation of the SEC necessarily means that $m_d > m_{d,crit}$. So, one interesting possibility is that the final fate of the black hole depends only on the dilaton coupling for general matter fields if the SEC holds.

For $\gamma \geq 1$, interesting behavior can be expected when m_d is slightly below $m_{d,crit}$. In this case, the temperature approaches zero by reducing the mass. However, there is a local maximum of $1/T$ in the M-$1/T$ diagram, as we can see in Figs. 2 and 4. So we may find a rapid evaporation below some gravitational mass.

Related to the above discussion, one may wonder whether the extreme solution is a numerical artifact. That is, although the temperature approaches zero by reducing the mass, it may have a local maximum in the M-$1/T$ diagram even in the case $m_d < m_{d,crit}$. To check this, we should rule out the possibility that we might have stopped the calculation before a local maximum in the M-$1/T$ diagram appeared [12]. We do this in the next section.

V. NEAR CRITICAL DILATON MASS

Here, we show the qualitative difference caused by the dilaton mass in a more explicit way. We do this by means of a diagram for the case $\gamma = 1$. However, our discussion is general for arbitrary γ.

In Sec. IV, we noted that there is an extreme solution for $m_d > m_{d,crit}$. This becomes more clear if the existence of the inner horizon and its merger with the

event horizon in the extreme limit can be demonstrated. We plot the event horizon r_h as a function of the gravitational mass M of the massive dilaton black hole for $\gamma = 1$ near $m_{d,crit}$ in Fig. 5 (solid lines). We also show the "inner horizon" with dotted lines.

As was shown in previous papers [8], there is no "inner horizon" for large black holes, while one does appear for small black holes. This kind of behavior is also found in charged black holes with Born-Infeld type nonlinear electrodynamics [13]. It is also worth mentioning that the inner horizon disappears in the Born-Infeld type black hole if we include a dilaton field [14].

Since we need fine-tuning of the dilaton field ϕ to satisfy regularity at the inner horizon, a curvature singularity appears there in general and is spacelike as in the GM-GHS solution.

The "inner horizon" disappears below the point B in Fig. 5 where $dr_h/dM \to \infty$ and $r_h \sim 1/m_d$. The point A corresponds to the point where two horizons separate. Thus, this diagram supports our contention that there is an extreme solution for $m_d > m_{d,crit}$.

Thus, it is astonishing that there are solutions below points C for $14.8 \gtrsim m_d > m_{d,crit}$. In our calculation, gravitational mass of the point C coincides with that of the point A. So it is supposed that uniqueness of solutions for fixed parameters holds in our system. Temperature is finite and the SEC holds in these cases. The reason why solutions below points C exist for $14.8 \gtrsim m_d > m_{d,crit}$ is under investigation.

As m_d approaches $m_{d,crit}$ for $m_d > m_{d,crit}$, the curve between A and B becomes small. For $m_d = 13.6$, A almost coincides with B and C. It is natural to suppose that A coincides with B and C for $m_d = m_{d,crit}$. This is related to the existence of a triply-degenerate horizon, as pointed out in previous papers [8].

Finally, we investigate the properties of ϕ_h for various horizon radii, since ϕ_h cannot be determined analytically, and whether or not this quantity diverges is the key to the existence of the extreme solution, as discussed in Sec.IV.

Let us first examine the condition on ϕ_h for the existence of the regular horizon. From Eqs. (10) and (13), we obtain

$$\frac{r_h^4 m_d^2}{Q_m^2} < \frac{\gamma}{\phi_h} e^{-2\gamma\phi_h}, \qquad (32)$$

$$\frac{r_h^4 m_d^2}{Q_m^2} < \frac{1}{\phi_h^2}\left(\frac{r_h^2}{Q_m^2} - e^{-2\gamma\phi_h}\right) \qquad (33)$$

by requiring that $m_h' < 1/2$ and $\phi_h' < 0$, respectively. $\phi_h' < 0$ is required if ϕ is to decrease monotonically. We find from Eq. (32) that $\phi_h r_h$ must converge to zero for the existence of the $r_h \to 0$ limit.

A plot of r_h-$\phi_h r_h^3$ for $\gamma = 1$ is shown in Fig. 6. We find that $\phi_h r_h^3$ increases as r_h decreases when the horizon is large enough to satisfy $r_h > 1/m_d$.

On the other hand, when the horizon becomes too small to satisfy $r_h < 1/m_d$, then $\phi_h r_h^3$ decreases as r_h

decreases. Note that the curves for $m_d < m_{d,crit}$ approach those of the GM-GHS solution as r_h decreases.

For $m_d = 20$, we can safely conclude that, since $\phi_h r_h^3$ monotonically increases but does not diverge as r_h decreases, $m_h' = 1/2$ is satisfied for a nonzero horizon radius. For $m_d = 15$, no conclusion can be drawn from this diagram.

To judge whether or not the extreme solution is realized exactly for nonzero horizon radius, we need to investigate the behavior of $\phi_h r_h$ for dilaton masses near $m_{d,crit}$ ($m_d = 13 \sim 14$) as shown in Fig. 7. Since $\phi_h r_h$ increases monotonically as r_h decreases for $m_d = 13.6$ and 14, we can conclude that $m_h' = 1/2$ is satisfied for a nonzero horizon radius. Thus, the black hole properties change at $m_{d,crit}$, as shown by the behavior of ϕ_h.

VI. CONCLUSION AND DISCUSSION

We have investigated static spherically symmetric solutions in the Einstein-Maxwell-dilaton system with a dilaton potential $V = m_d^2 \phi^2$. We considered the magnetically charged solution for various values of the dilaton coupling. We confirmed that the properties of black holes change qualitatively at $m_{d,crit}$.

For $m_d \geq m_{d,crit}$, which means the violation of the SEC, there is an extreme solution for nonzero horizon radius. For $m_d < m_{d,crit}$, the solution continues to exist in the $r_h \to 0$ limit where the temperature remains either finite and nonzero, diverges, or approaches zero for $\gamma = 1$, $\gamma > 1$ and $\gamma < 1$, respectively.

This property may also hold when the SEC is not violated. For example, the Einstein-Yang-Mills-dilaton (EYMD) system has been considered before [3–5] and exhibits thermodynamic properties similar to those above, if the black hole has a globally magnetic (or electric) charge. To prove this for general matter fields, or to find a counterexample is a task we hope to take up in future research.

ACKNOWLEDGMENTS

[1] G. W. Gibbons and K. Maeda, Nucl. Phys. B **298**, 741 (1988); D. Garfinkle, G. T. Horowitz and A. Strominger, Phys. Rev. D **43**, 3140 (1991).

[2] For the notation, see our action (1).

[3] G. Lavrelashvili and D. Maison, Nucl. Phys. B **410**, 407 (1993); E. E. Donets and D. V. Gal'tsov, Phys. Lett. B **302**, 411 (1993); T. Torii and K. Maeda, Phys. Rev. D **48**, 1643 (1993); C. M. O'Neill, Phys. Rev. D **50**, 865 (1994).

[4] B. Kleihaus, J. Kunz and A. Sood, Phys. Lett. B **354**, 240 (1995); *ibid.*, Phys. Rev. D **54**, 5070 (1996); *ibid.*, Phys. Lett. B **372**, 204 (1996); *ibid.*, **374**, 289 (1996); *ibid.*, **418**, 284 (1998).

[5] T. Tamaki, K. Maeda and M. Inada, Phys. Rev. D **63**, 087504 (2001).

[6] T. Tamaki, K. Maeda and T. Torii, Phys. Rev. D **57**, 4870 (1998); *ibid.*, **60**, 104049 (1999).

[7] C. Will, Theory and Experiment in Gravitational Physics (Cambridge Univ. Press, Cambridge, 1981).

[8] R. Gregory and J. A. Harvey, Phys. Rev. D **47**, 2411 (1993); J. H. Horne and G. T. Horowitz, Nucl. Phys. B **399**, 169 (1993).

[9] As for the classification of solutions in the Einstein-Maxwell system, see [10].

[10] K. G. Zloshchastiev, Phys. Rev. D **64**, 084026 (2001).

[11] T. Tamaki and H. Yajima, Phys. Rev. D **64**, 084002 (2001).

[12] Actually in [11], we misjudged some cases which have a solution in the $r_h \to 0$ limit as cases in which there is an extreme solution.

[13] M. Demianski, Found. Phys. **16**, 187 (1986); H. d' Oliveira, Class. Quant. Grav. **11**, 1469 (1994).

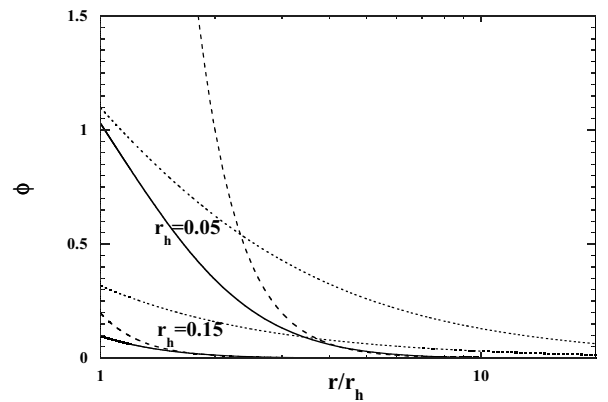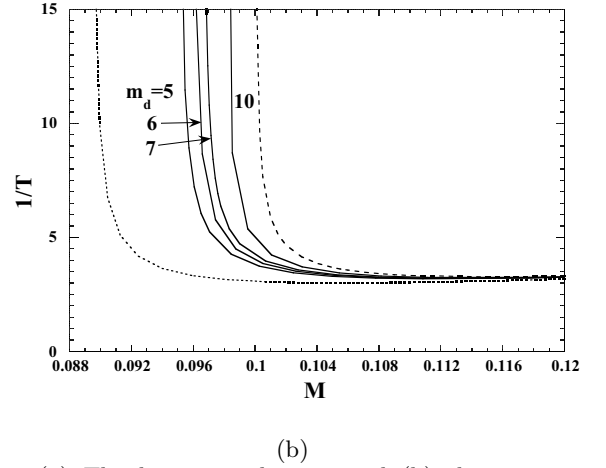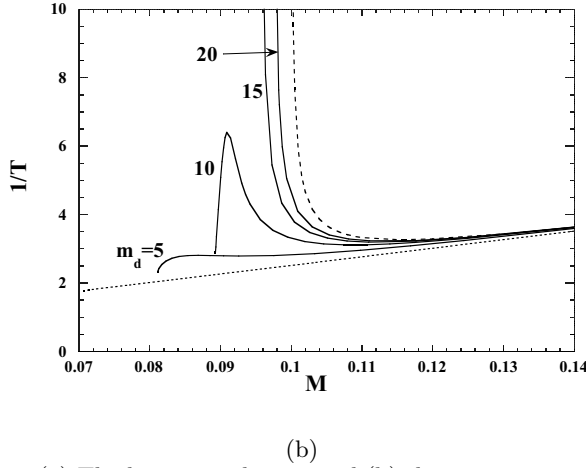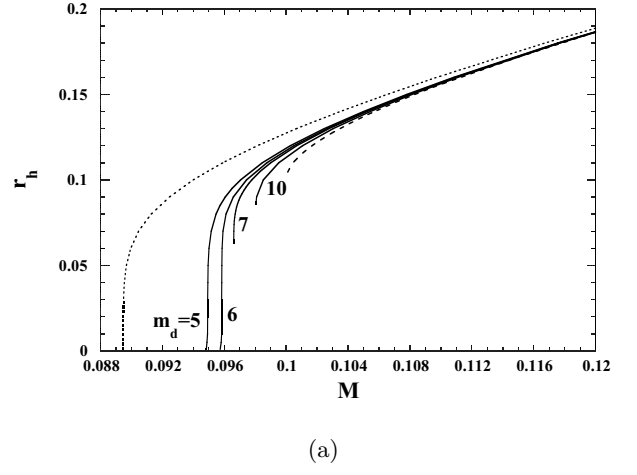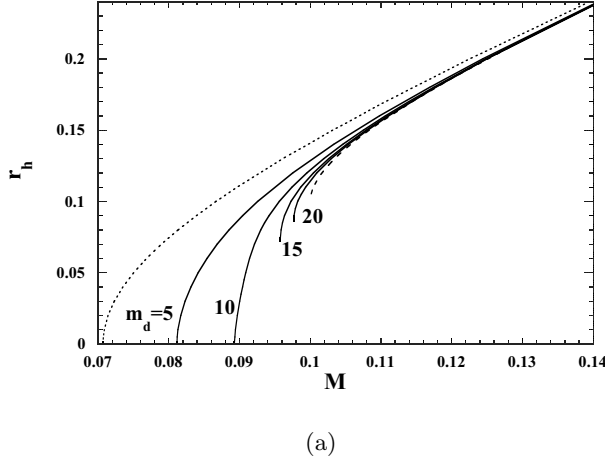[14] T. Tamaki and T. Torii, Phys. Rev. D **62**, 061501 (2000); *ibid.*, **64**, 024027 (2001).

FIG. 1. The behavior of the dilaton field with $\gamma = 1$ for $m_d = 0$, 10 and the approximate solution are shown with dotted lines, solid lines and dashed lines, respectively.
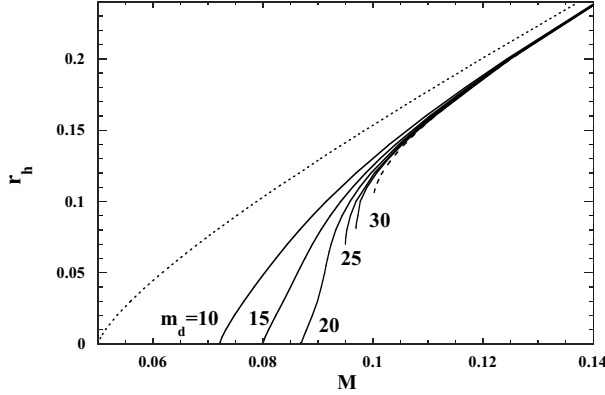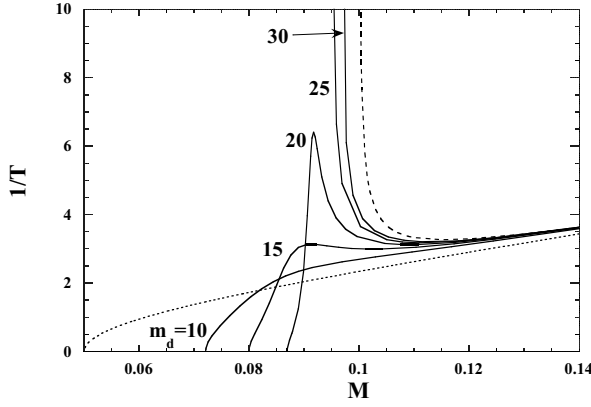
(a)

(b)

FIG. 2. (a) The horizon radius r_h and (b) the inverse temperature $1/T$ in terms of the gravitational mass M with $\gamma = 1$. The massive solution, GM-GHS solution and RN solution are plotted as solid lines, as dotted lines, and a dashed line, respectively.

(a)

(b)

FIG. 3. (a) The horizon radius r_h and (b) the inverse temperature $1/T$ in terms of the gravitational mass M with $\gamma = 0.5$. The massive solution, GM-GHS solution and RN solution are plotted as solid lines, as dotted lines, and a dashed line, respectively.
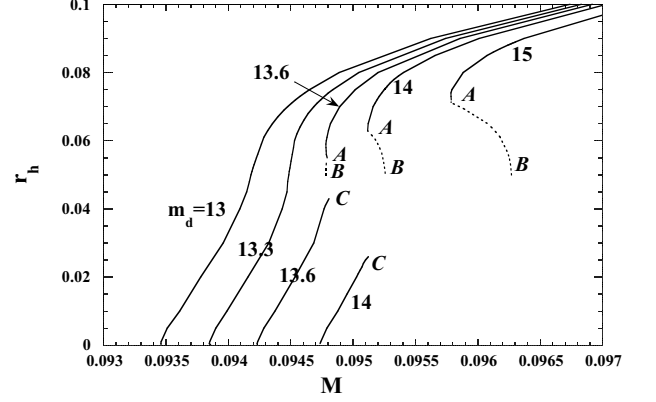
(a)

(b)

FIG. 4. (a) The horizon radius r_h and (b) the inverse temperature $1/T$ in terms of the gravitational mass M with $\gamma = \sqrt{3}$. The massive solution, GM-GHS solution and RN solution are plotted as solid lines, as dotted lines, and a dashed line, respectively.

FIG. 5. The horizon radius r_h as a function of the gravitational mass M with $\gamma = 1$.
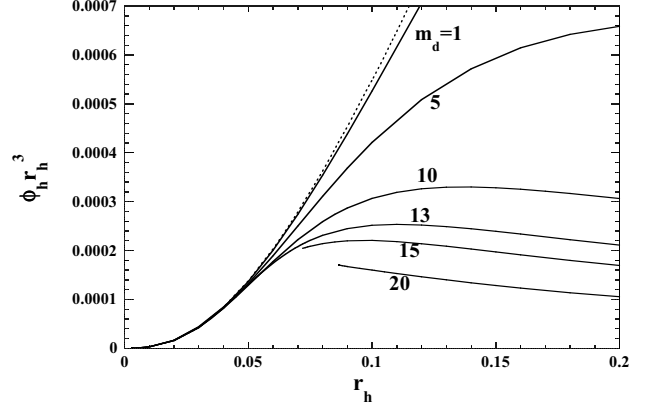

FIG. 6. The relationship between r_h and $\phi_h r_h^3$ for $\gamma = 1$ (shown also for the GM-GHS solution as a dotted line.).
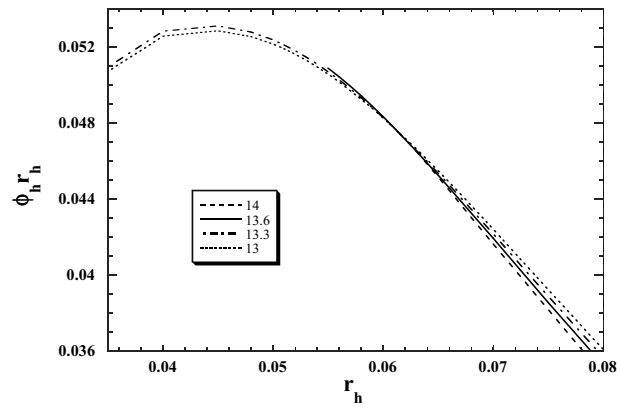
FIG. 7. The relationship between r_h and $\phi_h r_h$ for $\gamma = 1$.